Retrocyclin-2: Structural Analysis of a Potent Anti-HIV θ-Defensin[†,‡]

Norelle L. Daly,[§] Yi-Kuang Chen,[§] K. Johan Rosengren,[§] Ute C. Marx,[§] Martin L. Phillips,[||] Alan J. Waring,[⊥] Wei Wang,[⊥,#] Robert I. Lehrer,[⊥] and David J. Craik*[,§]

Institute for Molecular Bioscience and Australian Research Council Special Research Centre for Functional and Applied Genomics, The University of Queensland, Brisbane QLD 4072, Australia, Department of Chemistry and Biochemistry, UCLA, Los Angeles, California 90095, and Department of Medicine, David Geffen School of Medicine at UCLA, Los Angeles, California 90095

Received April 17, 2007; Revised Manuscript Received June 21, 2007

ABSTRACT: Retrocyclins are circular mini-defensins with significant potential as agents against human immunodeficiency virus, influenza A, and herpes simplex virus. Retrocyclins bind carbohydrate-containing surface molecules such as gp120 and CD4 with high affinity (K_d, 10−100 nM), promoting their localization on cell membranes. The structural features important for activity have yet to be fully elucidated, but here, we have determined the first three-dimensional structure of a retrocyclin, namely, one of the most potent forms, retrocyclin-2. In the presence of SDS micelles, a well-defined β-hairpin braced by three disulfide bonds that defines the cystine ladder motif is present. By contrast, a well-defined structure could not be determined in aqueous solution, suggesting that the presence of SDS micelles stabilizes the extended conformation of retrocyclin-2. Translational diffusion measurements indicate that retrocyclin-2 interacts with the SDS micelles, and such a membrane-like interaction may be an important feature in the mechanism of action of these antimicrobial peptides. Analytical ultracentrifugation and the NMR data indicated that retrocyclin-2 self-associates to form a trimer in a concentration-dependent manner. The ability to self-associate may contribute to the high-affinity binding of retrocyclins for glycoproteins by increasing the valency and enhancing the ability of retrocyclins to cross-link cell surface glycoproteins.

Retrocyclins are circular peptides with broad spectrum antimicrobial properties that can protect cells from infection by HIV-1[1] (*1*−*4*), herpes simplex (*5*), and influenza A (*6*) viruses. Recently, it has been reported that retrocyclins are also effective against *Bacillus anthracis* and that they may provide novel molecular templates for designing agents effective against *B. anthracis* and its toxins (*7*). Retrocyclins are promising antiretroviral preventatives (*8*) and belong to a family of proteins known as defensins, which are host defense peptides containing three disulfide bonds within a largely β-sheet structure.

Three subfamilies of defensin peptides with different disulfide connectivities exist in vertebrates. Despite differences in cysteine pairings, the α- and β-defensins share a similar overall fold, with a central triple stranded β-sheet stabilized by cross-bracing disulfide bonds. The θ-defensins (including retrocyclins) were discovered only recently (*9*) and have received less study than the α- and β-defensins. The original θ-defensin, RTD-1, was detected in leukocytes obtained from the rhesus monkey (*9*), contains 18 residues, and has a circular backbone. Intriguingly, the *in vivo* biosynthetic formation of its circular backbone involves the ligation of two 9-residue peptides, each derived from the C-terminal domain of a prepropeptide that is encoded by a θ-defensin (DEFT) gene, as schematically represented in Figure 1. Human bone marrow expresses mRNA that is homologous to the precursors of the rhesus monkey minidefensins (*1*), but a premature stop codon within the signal sequence domain of the human mRNA transcripts prevents translation. θ-defensin peptides are therefore considered to represent expressed pseudogenes. At least, six DEFT pseudogenes (DEFTΨ) are present in the human genome, all containing the premature stop codon in their signal sequence. Phylogenetic studies indicate that the putative ancestral human circular minidefensin was lost by a mutation that occurred in a common ancestor of gorillas, chimpanzees, and humans (*10*).

Synthetic forms of the erstwhile human θ-defensins based on the human DEFT pseudogene sequences and the processing sites of RTD-1 (*1*) have been shown to confer protection against HIV-1 infection (*5*). As well as having broad-spectrum anti-viral activity, retrocyclins exhibit lectin-like binding to carbohydrate-containing surface molecules includ-

[†] The NMR studies were supported in part by a grant from the University of Queensland Foundation (to N.L.D.) and the Australian Research Council (to D.J.C.). The studies were also supported, in part, by a grant to R.I.L. from the National Institutes of Health (AI056921). N.L.D. is a NHMRC Industry Fellow. D.J.C. is an ARC Professorial Fellow.

[‡] The retrocyclin-2 structures have been deposited in the Protein Data Bank with the code 2ATG, and the chemical shifts have been deposited at the BioMagResBank with the accession number 6815.

* Corresponding author. Phone: 61-7-3346 2019. Fax: 61-7-3346 2029. E-mail: d.craik@imb.uq.edu.au.

[§] The University of Queensland.

[||] Department of Chemistry and Biochemistry, UCLA.

[⊥] Department of Medicine, David Geffen School of Medicine at UCLA.

[#] Current address: Amgen, Thousand Oaks, CA.

[1] Abbreviations: DEFT, θ-defensin gene; HIV, human immunodeficiency virus; HPLC, high performance liquid chromatography; NMR, nuclear magnetic resonance; RTD-1 Rhesus theta defensin-1, SDS, sodium dodecylsulfate.

10.1021/bi700720e CCC: $37.00
Published on Web 08/08/2007

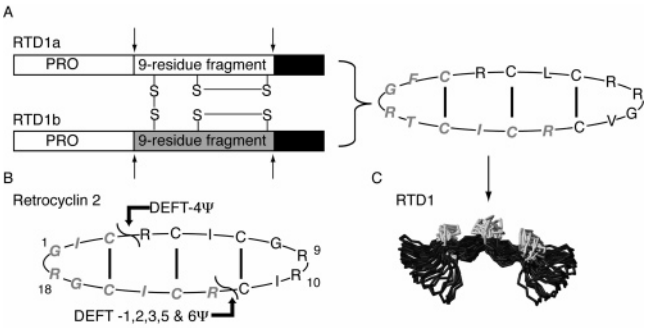

FIGURE 1: Gene structure and sequences of θ-defensins. (A) θ-Defensin RTD-1 biosynthesized from two 9-residue peptides that are oxidized and seamlessly ligated to form an 18-residue peptide that contains three disulfide bonds (*9*). The two 9-residue fragments are distinguished in the cyclic representation by black lettering for fragment 1 and gray italic lettering for fragment 2. (B) Sequence of retrocyclin-2. Residue numbering corresponds to the sequence of the linear retrocyclin-2 octadecapeptide that was prepared by solid-phase synthesis. The putative *in vivo* processing sites in ancestral retrocyclin are indicated with black arrows and also indicated are the human DEFTΨ pseudogenes that encode the respective nonapeptide domains incorporated into synthetic retrocyclin-2. Six θ-defensin genes have been found in the human genome, with DEFTΨ 1, 2, 3, 5, and 6 encoding an identical nonapeptide sequence and DEFTΨ 4 encoding a sequence differing only by one residue compared to the other five genes (*10*). (C) Solution structure of RTD-1 calculated using NMR spectroscopy PDB ID code 1HVZ (*13*). The cysteine residues are shown in gray and the backbone in black.

ing gp120 and CD4 (*11*) and represent the first such molecules to be identified in vertebrates. The ability of retrocyclins to recognize and bind carbohydrate-containing surface molecules (*11*) and to interfere with 6-helix bundle formation by binding to heptad repeat-2 of gp41 (*12*) is integral to their ability to protect cells from HIV-1 infection. Given their potent anti-viral activity, unusual cyclic backbone, and unique mode of biosynthesis, determination of the structural and biochemical properties of retrocyclins is of great importance.

Figure 1 shows the sequence of one of the most potent θ-defensins, retrocyclin-2, and highlights the processing sites on the basis of analogy with RTD-1 gene sequences. Despite the sequence similarities, RTD-1 is not as potent as retrocyclin-2 against certain strains of HIV (*4*). Furthermore, a recent study indicated that retrocyclin-2 formed more stable complexes with gp120 and CD4 than any others of a range of θ-defensins tested (*4*). The implications of these functional differences from a structural perspective have not been explored, and the only structural information currently available for θ-defensins is on RTD-1. RTD-1 has a β-hairpin structure that shows disorder in the ensemble of NMR structures because of apparent flexibility (*13*) (Figure 1), but no three-dimensional (3D) structural information has been reported for the retrocyclins.

In the current study, we have determined the tertiary structure of retrocyclin-2 (Figure 1) in a membrane-mimicking environment and show that a well-defined β-hairpin structure is present. Furthermore, analytical ultracentrifugation and NMR experiments indicate that retrocyclin-2 self-associates to form a trimer in a concentration-dependent manner. These structural data provide a foundation for future studies to decipher structure−activity relationships of this exciting new class of anti-microbial, anti-viral, and anti-toxic agents.

EXPERIMENTAL PROCEDURES

Peptide Synthesis, Folding, and Purification. The linear sequence of retrocyclin-2 was prepared on a 0.25 mmol scale with an ABI 431A peptide synthesizer using FastMoc chemistry (*14*) as previously described (*1*, *11*). After cleavage and deprotection of the peptide from the resin using trifluoroacetic acid/1,2-ethanedithiol/thioanisole/water, 10:0.25:0.5:0.5 (v/v) (*15*), the peptide was separated from the resin by filtration and precipitated from solution with tertiary butyl ether. The crude material was purified by reverse phase HPLC using a Vydac C18 column. This purified reduced peptide was then oxidized in buffer, followed by separation of the oxidized peptide from unreacted peptide with HPLC (*1*). The oxidized peptide then was cyclized in DMSO with 1-ethyl-(3-dimethylaminopropyl)carbodiimide and *N*-hydroxbenzotriazole (*1*). The cyclized peptide derivative was then separated from any remaining non-cyclized material by preparative RP-HPLC similar to that used for purification of the reduced peptide.

NMR Spectroscopy. Samples for ^{1}H NMR measurements contained 0.6 to 4 mM peptide in 90% H_2O/10% ^2H_2O (v/v), 100 mM SDS 90% H_2O/10% ^2H_2O (v/v), 10% acetonitrile/80% H_2O/10% ^2H_2O, 10 mM phosphate buffer at pH 7.4 in 10%^2H_2O, or 90% methanol/10% ^2H_2O at pH 3−6. Spectra were recorded at 285−315 K on Bruker Avance-500 or Bruker Avance-600 spectrometers. 2D NMR spectra were recorded in phase-sensitive mode using time-proportional phase incrementation for quadrature detection in the t_1 dimension (*16*). The 2D experiments included TOCSY (*17*) using a MLEV-17 spin−lock sequence (*18*) with a mixing time of 80 ms and DQF-COSY (*19*), ECOSY (*20*), and NOESY (*21*) with mixing times of 100−250 ms. Solvent suppression was achieved using a modified WATERGATE sequence (*22*). Spectra were acquired over 6024 Hz with 4096 complex data points in F_2 and 512 increments in the F_1 dimension. $^3J_{HN-H\alpha}$ coupling constants were measured from a one-dimensional (1D) spectrum or from the DQF-COSY spectrum. Spectra were processed on a Silicon Graphics Octane workstation using XWINNMR (Bruker) software. The t_1 dimension was zero-filled to 1024 real data points, and 90° phase-shifted sine bell window functions were applied prior to Fourier transformation. Chemical shifts were referenced to internal 2,2-dimethyl-2-silapentane-5-sulfonate.

Pulsed-field-gradient NMR diffusion experiments were performed with a 2D sequence using stimulated echo longitudinal encode−decode (*23*). The lengths of all pulses and delays were held constant and 32 spectra acquired, with the strength of the diffusion gradient varying between 2% and 95% of the maximum value. The lengths of the diffusion gradient and the stimulated echo were optimized for each sample to give a total decay in the protein signal of ~90%. The data were analyzed using the software package Topspin (Bruker). Using dioxane (0.2 mM) as an internal standard, with an effective hydrodynamic radius of 2.12 Å, the hydrodynamic radii of the retrocyclin-2 samples were calculated using a published equation (*24*). Errors in the hydrodynamic radii were calculated on the basis of the observed deviations in the fits for the diffusion coefficients.

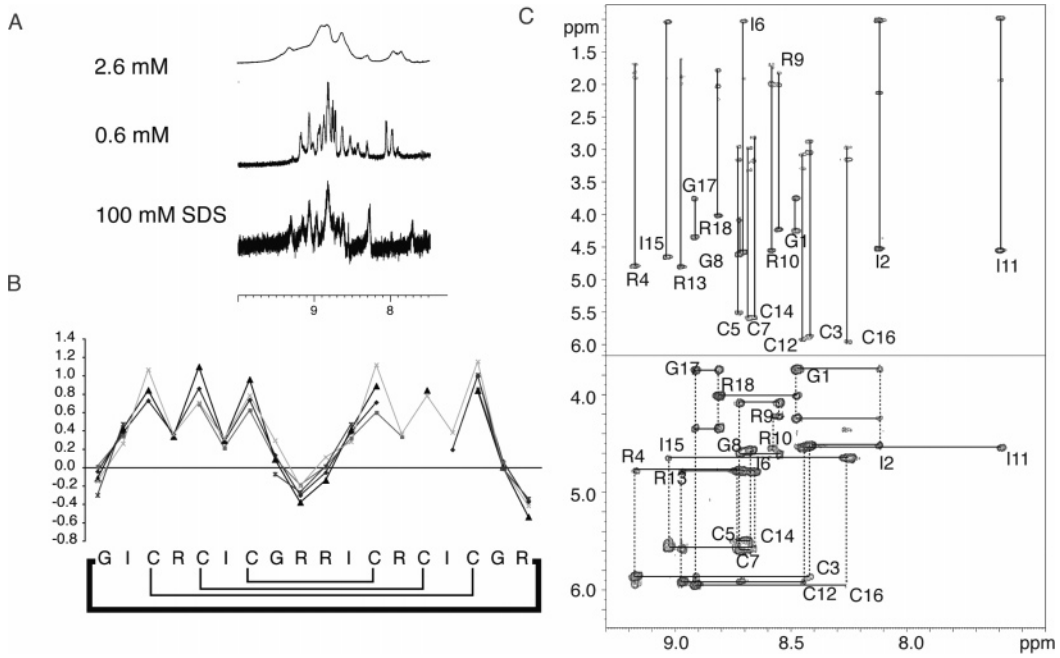

FIGURE 2: NMR data for retrocyclin-2. (A) One-dimensional 600 MHz NMR spectra of retrocyclin-2 recorded for 0.6 mM peptide in 95% H_2O/5% D_2O and 2.6 mM peptide in 95% H_2O/5% D_2O. (B) Secondary shifts determined by subtracting the random coil shift (*43*) from the observed αH shift. The solution conditions are as follows: 10% acetonitrile (♦); 90% methanol (▲); water 0.6 mM (■); water 2.6 mM (★); 100 mM SDS (×). The peptide concentration is 0.6 mM for methanol and SDS conditions but 1.3 mM in acetonitrile. (C) Regions of the TOCSY (top) and NOESY (bottom) spectra for retrocyclin-2 in 100 mM SDS.

Structure Calculations. Preliminary structures of retrocyclin-2 were calculated using a torsion angle simulated annealing protocol within the program DYANA (*25*). Final structures were calculated using simulated annealing and energy minimization protocols within CNS version 1.1 (*26*). The starting structures were generated using random (ϕ, ψ) dihedral angles and were energy-minimized to produce structures with the correct local geometry. A set of 50 structures was generated by a torsion-angle-simulated annealing protocol (*27*, *28*). Disulfide bond restraints were included on the basis of analogy with RTD-1. This protocol involves a high-temperature phase comprising 4000 steps of 0.015 ps of torsion-angle dynamics, a cooling phase with 4000 steps of 0.015 ps of torsion-angle dynamics, and finally an energy-minimization phase comprising 500 steps of Powell minimization. Structures consistent with restraints were subjected to further molecular dynamics and energy minimization in a water shell, as described by Linge and Nilges (*29*). The refinement in explicit water involves the following steps. First, heating to 500 K via steps of 100 K, each comprising 50 steps of 0.005 ps of Cartesian dynamics. Second, 2500 steps of 0.005 ps of Cartesian dynamics at 500 K before a cooling phase where the temperature is lowered in steps of 100 K, each comprising 2500 steps of 0.005 ps of Cartesian dynamics. Finally, the structures were minimized with 2000 steps of Powell minimization. Structures were analyzed using PROMOTIF (*30*) and PROCHECK-NMR (*31*). The structures have been deposited in the protein data bank with the code 2ATG.

Ultracentrifugation. Sedimentation equilibrium runs were performed at 25 °C on a Beckman Optima XL-A analytical ultracentrifuge in 12 mm path length double sector cells. All samples were in 100 mM NaCl and 10 mM Tris at pH 7.4. Absorption was monitored at 228 nm for 0.05 mM samples and at 260 nm for 0.5 mM samples. Sedimentation equilibrium profiles were measured at 40,000 and 50,000 rpm. The data were initially fitted with a nonlinear least-squares exponential fit for a single ideal species using the Beckman Origin-based software (Version 3.01). Preliminary analysis of the association behavior used the global analysis software (the multifit option of the above-mentioned software) to analyze four scans simultaneously, corresponding to protein at 0.05 mM at 40,000 and 50,000 rpm, and protein at 0.5 mM at 40,000 and 50,000 rpm. Partial specific volumes were calculated from the amino acid composition (*32*).

RESULTS

Retrocyclin-2 was synthesized and purified as previously described (*1*, *11*). NMR spectra were recorded under a range of conditions, as shown in Figure 2. At millimolar concentrations in aqueous solution, broad spectral peaks were observed, consistent with oligomers being present or there being exchange broadening due to equilibration between two or more conformational states. Decreasing the concentration from 4 to 0.5 mM in water significantly improved the NMR spectra, with much sharper lines observed, consistent with concentration-dependent self-association. By contrast, at 0.5 mM in phosphate buffer, broad lines were still evident. Given the reported propensity for retrocyclins to interact with lipid bilayers (*33*), spectra were also recorded under hydrophobic conditions, including in the presence of SDS micelles and 10% acetonitrile.

Sequential assignments of the NMR spectra were determined using TOCSY and NOESY spectra, and the secondary shifts (i.e., the differences between observed chemical shifts and values for the corresponding residue in a random coil peptide) are given in Figure 2 for a range of solution conditions. At high concentration in aqueous solution, only partial assignments were possible because of the particularly large broadening of the cysteine residues. Nonetheless, a

comparison of the secondary shifts reveals minimal differences, indicating that no significant structural changes occur over the range of solution conditions examined. The NMR secondary shifts suggest the presence of two clearly defined β-strands (residues 3−8 and 11−16) separated by turn regions.

Despite the similar secondary shifts under different solution conditions, the largest number of NOEs and the best dispersion of the amide proton chemical shifts of the cysteine residues were observed in the presence of membrane-mimicking SDS micelles. Initial structure calculations were performed on the basis of the data recorded at low concentration in aqueous solution, but insufficient NOEs were present to define the structure. Thus, the SDS micelle solution environment was chosen for determining the 3D structure of retrocyclin-2. The amide regions of the TOCSY and NOESY spectra of retrocyclin-2 recorded in the presence of SDS micelles are given in Figure 2.

Prior to calculating the structure, it was of interest to determine whether retrocyclin-2 directly interacted with the SDS micelles or whether the improved spectral properties simply reflected a solution dielectric effect or other nonspecific phenomenon. This was achieved by determining the effective hydrodynamic radius of retrocyclin-2 using NMR pulsed-field-gradient diffusion experiments. This technique has been successfully applied to a range of peptides and proteins to monitor the effective size of molecular complexes (*23*, *24*). A solution of 100 mM SDS in the absence of retrocyclin-2 was used as a control and gave a hydrodynamic radius of 21.5 ± 1.2 Å, consistent with dynamic light-scattering measurements (*34*). In the presence of 100 mM SDS, the calculated radius for retrocyclin-2 is significantly increased to 28.7 ± 1.7 Å, whereas in aqueous solution, it was between 12.6 and 15.1 Å depending on the conditions. These results clearly indicate that retrocyclin-2 strongly interacts with SDS micelles.

Elucidation of the 3D structure of retrocyclin-2 in the presence of SDS micelles revealed that the structure is better defined in this environment than in water. Structures were calculated with 98 distance restraints and 13 dihedral angle restraints using a simulated annealing protocol in CNS. A superposition of the 20 lowest-energy structures and a ribbon representation of the secondary structure are shown in Figure 3. Geometric and energetic statistics are given in Table 1 and indicate a well-defined structure. The Ramachandran plot statistics are 74.3% in the most favored region, 22.5% in the additional allowed, and 3.2% in the generously allowed regions.

An analysis of the structures with PROMOTIF (*30*) shows that the main element of secondary structure of retrocyclin-2 is a β-hairpin, consistent with expectations from the NMR chemical shift, coupling, and NOE data. The strands of the β-hairpin comprise residues 3−8 and 11−16 connected by a β-turn from residues 8−11. The β-turn does not fit into one of the classical turn types, most likely because this region is slightly disordered. The other turn connecting the strands of the β-hairpin is an inverse γ-turn involving residues 17, 18, and 1. One face of the molecule is essentially made up of the side chains of the cysteine residues, whereas the other face comprises the side chains of the remaining residues, namely, isoleucine, arginine, and glycine. A comparison with two related cyclic disulfide-rich peptides is also given in Figure 3 to highlight the structural differences and similarities between several classes of recently discovered cyclic peptides.

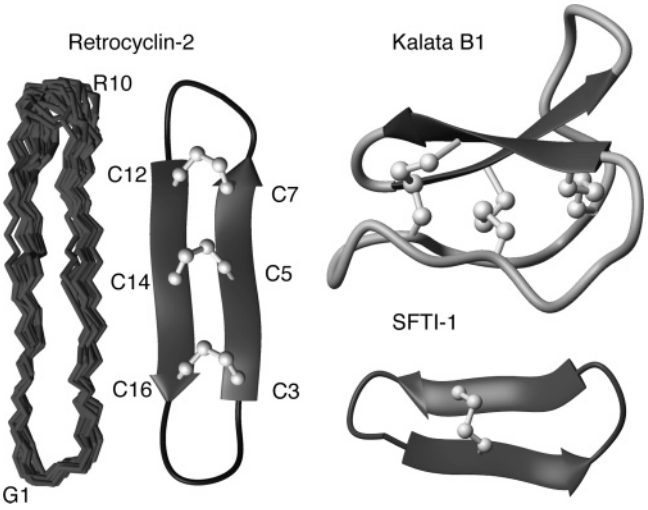

FIGURE 3: Three-dimensional structure of retrocyclin-2 in 100 mM SDS. A superposition of the 20 lowest energy structures is shown on the left of the diagram and the lowest energy structure shown with the β-strands as arrows and the disulfide bonds in ball and stick format in the bottom panel. This topology defines a cystine ladder structural motif. The structures of two other circular proteins are also shown for comparison, i.e., kalata B1 (*44*) and SFTI-1 (*39*).

Table 1: NMR and Refinement Statistics for Retrocyclin-2

NMR Distance and Dihedral Constraints	
distance constraints	
total NOE	98
intra-residue	41
inter-residue	57
sequential ($\|i - j\| = 1$)	37
medium-range ($\|i - j\| < 4$)	2
long-range ($\|i - j > 5$)	18
intermolecular	0
total dihedral angle restraints	
ϕ (restraints were implemented with ranges of ±30°)	13
Structure Statistics	
violations (mean and s.d.)	
distance constraints (Å)	0.05 ± 0.005
dihedral angle constraints (°)	1.18 ± 0.25
max. dihedral angle violation (°)	3
max. distance constraint violation (Å)	0.3
deviations from idealized geometry	
bond lengths (Å)	0.004 ± 0.0001
bond angles (°)	0.46 ± 0.03
impropers (°)	0.31 ± 0.04
average pairwise r.m.s.d.[a] (Å)	
heavy (residues 3−17)	2.16 ± 0.43
backbone (residues 3−17)	0.79 ± 0.29

[a] Pairwise rmsd was calculated among 20 refined structures.

An analysis of slowly exchanging amide protons after the dissolution of peptides in D_2O can give an indication of the hydrogen bonds present. Under the conditions used for calculating the structure of retrocyclin-2, these D_2O exchange experiments suggested that a number of amide protons were slowly exchanging, but low signal-to-noise prevented a complete analysis. However, the presence of intramolecular hydrogen bonds stabilizing the structure determined in SDS micelles is supported by the sensitivity of amide-proton chemical shifts to temperature. Temperature coefficients more positive than −4.6 ppb/K are generally indicative of hydro-

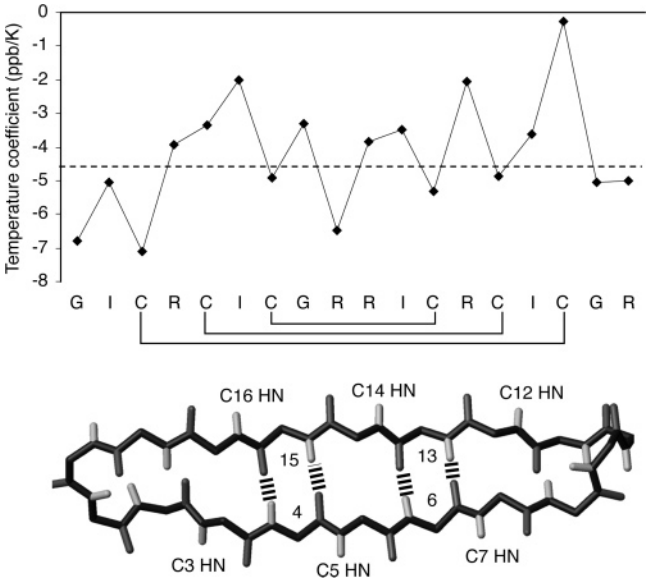

FIGURE 4: Amide temperature coefficients of retrocyclin-2 and 3D structure highlighting the amide proton locations. (A) TOCSY spectra recorded between 285 and 315 K and the changes in amide proton chemical shifts measured as a function of temperature, with the temperature coefficients derived from a linear regression analysis. The arbitrary cutoff defining hydrogen bonding of −4.6 ppb/K is shown as a dotted line. Amide protons showing temperature coefficients more positive than −4.6 ppb/K have a hydrogen bond predictivity value exceeding 85% (*35*). (B) Backbone atoms of the lowest energy structure, highlighting the fact that the Cys amide protons protrude from the structure and that the amide protons of Ile6 and Arg13 that are slowly exchanging at high concentration are ideally located to be involved in intramolecular hydrogen bonds.

gen bonds (*35*). Several residues in retrocyclin-2 in SDS micelles have temperature coefficients more positive than −4.6 ppb/K, particularly in the β-sheet region, as shown in Figure 4.

Following calculation of the 3D structure of retrocyclin-2, it was of interest to determine the nature of the self-association apparent from the increased line width at higher concentrations. This was achieved using analytical ultracentrifugation as well as by an NMR determination of translational diffusion coefficients. Analytical ultracentrifugation of retrocyclin-2 was performed in 100 mM NaCl and 10 mM Tris at pH 7.4 at speeds of 40,000 and 50,000 rpm. The weight-average molecular weight, determined by single-exponential fits to individual scans, was found to be speed- and concentration-dependent, strongly suggesting an associating system, as did the nonrandom nature of the residuals (Figure 5). The molecular masses varied from 2755 Da at 0.05 mM and 50,000 rpm to 5616 Da at 0.5 mM and 40,000 rpm. These correspond to 1.36 to 2.78 times the monomeric molecular weight of retrocyclin-2 (2018 Da). Group analysis of all four files (two concentrations at two speeds) using various models indicated that the data could be satisfactorily explained by either of two models, a monomer−trimer equilibrium or a monomer−dimer + monomer−tetramer (which is equivalent to a monomer−dimer, dimer−tetramer, and tetramer equilibrium). Since the latter model uses three exponentials to fit the data to get the same quality of fit as that of the monomer−trimer fit, which uses only two exponentials, it is not favored. The association constant derived from the analytical ultracentrifugation data for trimer formation is 3×10^8 M^{-2}. Similar results have recently been reported for retrocyclin-1 (*7*).

The NMR translational diffusion experiments correlate with the analytical ultracentrifugation experiments and highlight the influence of the solution conditions upon self-association. The diffusion measurements indicate that retrocyclin-2 at 0.5 mM has a hydrodynamic radius of 15.1 ± 0.9 Å in 10 mM phosphate buffer at pH 7.4. (The phosphate buffer was used because it is compatible with the NMR measurements.) The equation derived by Wilkins et al. (*24*) ($R_h = (4.75 \pm 1.11)N^{0.29\pm0.02}$, where N is the number of residues in the protein and R_h is the hydrodynamic radius in Angstroms) was used to estimate the oligomeric state of retrocyclin-2. This analysis indicated that trimers were present under these conditions, consistent with the results from analytical ultracentrifugation.

Analysis of the oligomeric state of retrocyclin-2 in the absence of buffer reveals that the solution conditions influence the state of oligomerization. A higher peptide concentration in water, compared to buffer, is required to observe the presence of predominately trimers. At 2.6 mM retrocyclin-2 in water, translational diffusion experiments indicate the presence of trimers, whereas at the lower concentration of 0.5 mM, a mixture of monomers and dimers or trimers was present. (That is, in the absence of buffer, the diffusion experiments indicate that there is a lower percentage of trimer present compared to that in the presence of buffer.) The difference between the oligomeric state of retrocyclin-2 under different solution conditions is not simply due to a decrease in pH because analysis of samples at different pH values in the absence of buffer did not result in a change in oligomerization state. Comparison of the 1D NMR spectra in the presence and absence of buffer reveals broadening of the peaks in the presence of buffer consistent with the formation of the trimer. From the analytical ultracentrifugation and translational diffusion experiments, it is clear that the solution conditions influence the state of oligomerization but that trimers predominate at 0.5 mM in the presence of buffer.

Further analysis of the 2D spectra of retrocyclin-2 recorded at higher concentration in aqueous solution provides additional information on the nature of the trimer. Given the similarity of chemical shifts across the range of conditions analyzed, the calculated 3D structure can be used to map the extent of broadening observed for various residues at higher concentrations. The TOCSY spectra recorded in aqueous solution at 2.6 mM retrocyclin-2 (i.e., a concentration where trimers predominate in water) have significantly broadened lines for the cysteine residues and broadening to a lesser extent for several other residues, and then the remainder of the residues are reasonably sharp, as shown in Figure 6. These three levels of broadening have been mapped onto the 3D structure calculated for retroyclin-2. It is clear that the cysteine residues occupy one face of the molecule and that the residues with the sharpest line width are located in the turn regions (Figure 6). The significantly increased broadening of the cysteine amide protons implies that they may be involved in an exchange process and are likely directly involved in interactions between monomers.

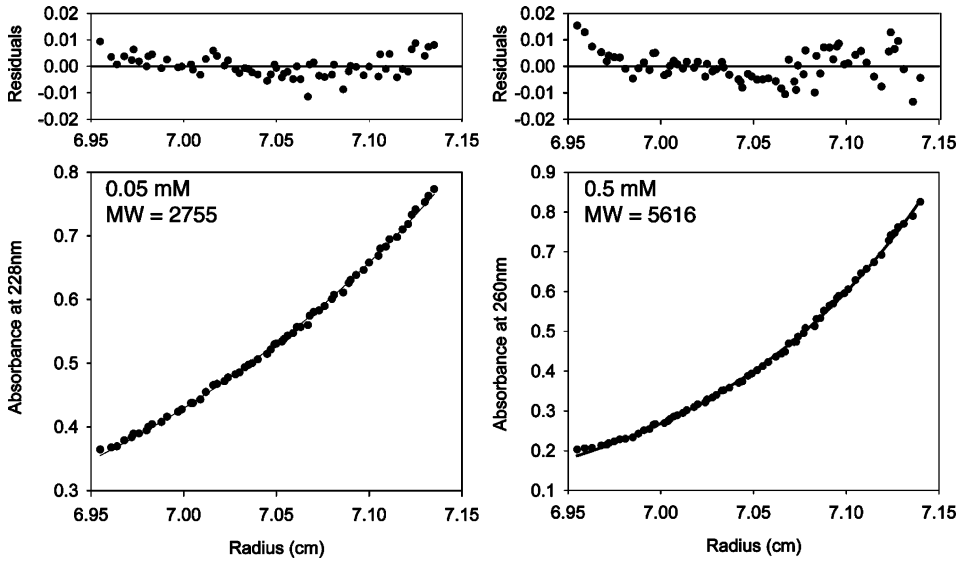

FIGURE 5: Sedimentation equilibrium studies on retrocyclin-2. Sedimentation equilibrium profiles of retrocyclin-2 and single-exponential fits to the data (which gives the weight-average molecular weight, which is also indicated). The weight-average molecular weights are strongly concentration dependent, indicating an associating system. The nonrandom nature of the residuals also indicates this equilibrium. Conditions of centrifugation were 25 °C, 40,000 rpm and a buffer of 100 mM NaCl, and 10 mM Tris at pH 7.4.

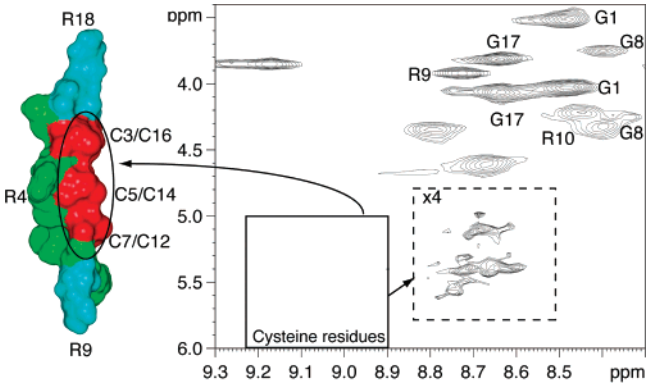

FIGURE 6: Selective broadening of the Cys residues in retrocyclin-2. (Right) Region of the TOCSY spectrum of retrocyclin-2 at a concentration of 2.6 mM in aqueous solution. Cysteine residues (solid box) are substantially broadened and invisible at the threshold displayed for the rest of the spectrum. The inset dotted box shows the cysteine residues at 4-fold magnification, using milder apodization functions to help with visualization. (Left) Extent of broadening of the cross-peaks mapped onto the surface of the 3D structure of retrocyclin-2. The cysteine residues are the most significantly broadened and are shown in red. Residues 2, 4, 6, 10, 11, 13, 15, and 16 are shown in green and display broadening but to a lesser degree than the cysteine residues, and residues 1, 8, 9, and 17 with relatively sharp peaks are shown in blue.

DISCUSSION

In the current study, we have determined the structure of retrocyclin-2 in the presence of membrane-mimicking micelles and shown that it associates with the micelles and forms a well-defined extended structure. In the absence of micelles, retrocyclin-2 self-associates in aqueous solution to form a trimer in a concentration-dependent manner. These biochemical properties of retrocyclin-2 may have implications for its biological activity, and in particular, the self-association tendency may contribute to its high-affinity binding to glycoproteins and its ability to inactivate the enzymatic activity of lethal factor, a secreted toxin of *Bacillus anthracis* (*7*).

Analysis of the αH secondary NMR shifts of retrocyclin-2 over a range of conditions indicated that a β-sheet structure is typically present. Determination of the 3D structure in aqueous solution was not possible because of a lack of NOEs. However, in the presence of SDS micelles, an extended β-sheet structure is stabilized (Figure 3). One face of the molecule essentially contains the side chains of the cysteine residues, with the side chains of the other residues on the other face of the molecule. The structure comprises a laddered arrangement of three disulfide bonds within the β-hairpin structure. We refer to this topological arrangement as a cystine ladder, as is apparent from Figure 4.

The laddered disulfide bond arrangement in the θ-defensins retrocyclin-2 and RTD-1 represents the simplest possible tri-disulfide connectivity within a circular backbone and contrasts with the knotted structure seen in the only other known cyclic tri-disulfide topology exemplified by the cyclotides (Figure 3) (*36*). Cyclotides are plant-derived anti-HIV peptides that contain a cystine knot (*37*) rather than a cystine ladder within their circular peptide backbone. The cystine knot effectively represents the most complex topological arrangement of three disulfide bonds, and it is interesting that the two extreme topologies (knotted and laddered) of disulfide bonds within macrocyclic peptides have now been reported, but intermediate topologies have so far not been seen. SFTI-1 is another circular protein, also isolated from plants, that has a β-sheet structure similar to that of retrocyclin-2 but is only braced by a single disulfide bond (Figure 3) (*38*). In SFTI-1, an extensive hydrogen-bonding network is responsible for stabilizing the fold (*38*, *39*), whereas retrocyclin-2 appears to require an external environmental factor such as the presence of SDS to stabilize the fold.

In most respects, the structure of retrocyclin-2 is similar to that of RTD-1, the only other θ-defensin for which a structure has been reported (*13*). However, unlike RTD-1, whose structure appears to be quite flexible, the two turns at either end of retrocyclin-2 are well defined with respect to each other, and the laddered framework is relatively rigid.

The difference in flexibility most likely reflects the fact that the retrocyclin-2 structure was determined in the presence of membrane-mimicking micelles but the RTD-1 structure was determined in their absence. In future studies, it would be of interest to determine the structure of RTD-1 in the presence of a membrane mimic to confirm this hypothesis. The interaction of retrocyclin-2 with SDS is presumably mediated by the electrostatic attraction between the positively charged peptide and negatively charged micelles, as has been proposed for the interaction of RTD-1 with negatively charged lipids (*40*). Another difference appears to be in the oligomeric state of the two peptides. In aqueous solution, RTD-1 showed no signs of oligomerization at 1 mM (*13*) in contrast to the tendency for retrocyclin-2 to self-associate. It is not unusual for small differences in sequence to significantly affect the aggregation of protein structures in general.

Insight into the nature of the interaction of retrocyclin-2 with SDS micelles has been provided by a recent study examining the interaction of retrocyclin-2 with lipid bilayers (*33*). Tang et al. showed that retrocyclin-2 adopts a transmembrane orientation in DLPC bilayers but changes to a more in-plane orientation in thicker POPC bilayers (*33*). Given the relatively large size of the SDS micelles used in the current study, it appears likely that a more in-plane orientation of retrocyclin-2 occurs in SDS micelles.

The self-association observed for retrocyclin-2 was determined by analytical ultracentrifugation and NMR analysis at different peptide concentrations. The analytical ultracentrifugation results show that the peptide is mostly trimer at 0.5 mM but a mixture of species at lower concentrations. The NMR diffusion experiments also reveal the presence of a trimer at 0.5 mM but only in the presence of buffer. In the absence of buffer, it appears that there is a lower percentage of trimer present. These results suggest that in the presence of buffers the propensity for self-association is increased, presumably on the basis of the interactions between the positively charged arginine residues with negatively charged ions from the buffer/salts present.

The trimer formed for retrocyclin-2 clearly reflects a dynamic exchange regime based on the broadened lines observed in the NMR spectra, the unchanged (i.e., fast-exchange averaged) chemical shifts upon formation of the trimer, and a lack of intermolecular NOEs. Although, in general, discriminating between inter and intramolecular NOEs can be difficult, the covalent geometry of retrocyclin-2 facilitates this discrimination. The circular backbone, braced by three disulfide bonds, imposes significant constraints on the secondary structure of retrocyclin-2, but clearly all of the observed medium and long-range NOEs are consistent only with intramolecular cross-strand NOEs. NOEs that would be expected between β-strands of different molecules are clearly absent. A trimer with similar properties has recently been observed in a 17-residue β-hairpin peptide derived from ubiquitin (*41*). Although the sequence of this peptide is significantly different from retrocyclin-2 and does not contain cysteine residues, the oligomerization properties mirror what is observed for retrocyclin-2. For instance, the NMR lines broaden at higher concentrations, and sedimentation equilibrium measurements indicate that the oligomer is a trimer. Furthermore, despite the broadening observed, the chemical shifts remain unaltered, indicating that the assembled species is a trimer of β-hairpins. The authors concluded that there is a very small free-energy barrier to association once an encounter complex is formed, consistent with the lack of change in chemical shifts upon formation of the trimer (*41*). Clearly, this is similar to what is observed for retrocyclin-2 and suggests that these properties may be intrinsic to such small β-hairpin structures and that such oligomeric assembly may facilitate a range of functions.

How the monomers interact is an interesting question, and the cysteine residues appear to play a crucial role in the self-association process. In addition to the general broadening observed as concentration increases, peaks from the cysteine residues display selective broadening. A likely explanation is that the cysteine amide protons are at the interface between monomers in the self-associated complex and that they are involved in the exchange process between monomer units and the complex. Similar selective broadening has previously been shown to be the result of self-association for the N-terminal domain of the rat T-cell antigen CD2 (*42*). The selective nature of the broadening is consistent with a small and well-defined self-associated complex rather than a nonspecific larger aggregate. Support for the cysteine residues being involved in intermolecular contacts comes from analysis of the structures determined for retrocyclin-2 in the presence of SDS. The amide protons of the cysteine residues protrude from the structures as highlighted in Figure 4 and are therefore ideally positioned for intermolecular interactions. Although this structure was determined in SDS micelles, the chemical shift analysis suggests that the secondary structure of the monomer does not change over the range of conditions analyzed.

Given that the structures of the individual hairpins of retrocyclin-2 in the trimer are similar to that calculated for the monomer, it is interesting to evaluate the possible modes of self-association. Three possible models are illustrated in Figure 7. The arrangements shown in A and B are unlikely because changes in chemical shifts upon association would be expected but are not experimentally observed. Arrangement A is not symmetrical, and the middle hairpin would be expected to experience a different environment than the other two hairpins. Whereas in arrangement B, only small regions of the molecules interact, leading to the expectation that upon association the chemical shifts for only these regions would vary. Analysis of the broadening observed at higher concentration in aqueous solution suggests that as the cysteine residues are the most significantly broadened they are involved in the primary interaction between the monomers. Consequently, the most likely association model is where a circular arrangement of the monomers occurs, with the cysteine residues located in the trimer core, as depicted in Figure 7C. The temperature coefficient data lend support to this model because Cys5 and Cys16 have temperature coefficients indicative of involvement in hydrogen bonds. Hydrogen bonds between the cysteine amide protons that protrude from the core of the structure would be expected in such an arrangement of the monomers.

The current study raises the question, what is the potential role of self-association in the biological activity of retrocylin-2? Despite being the smallest natural lectins identified to date, θ-defensins have the ability to bind viral glycoproteins, such as gp120 of HIV-1 or gB2 of HSV-2, and cell-surface glycoproteins, such as CD4, with surprisingly high affinity

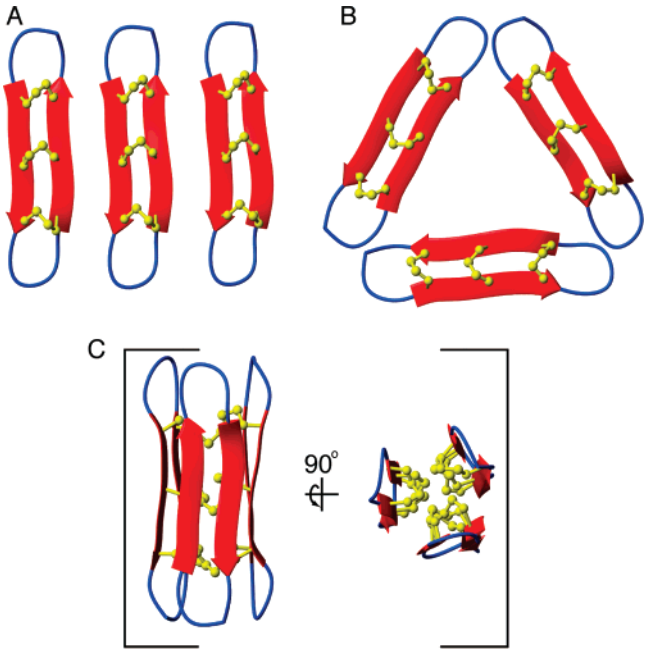

FIGURE 7: Possible trimer models for retrocyclin-2. The β-strands of each monomer are shown as arrows joined by the cyclic backbone. Three possible arrangements are depicted, but C appears to be the most likely one on the basis of the experimental results. Many more models for the trimer structures are potentially possible, but C best satisfies the symmetry requirements to be consistent with the chemical shift data.

(K_d, 10−100 nM). Their ability to form oligomers, substantiated by the data in this article, may play a key role in their high-affinity binding of glycoproteins by increasing the valency. Oligomer formation may be facilitated by binding to the glycoprotein and could also enhance the ability of retrocyclins to cross-link cell-surface glycoproteins.

A recent study suggested that the antiviral properties of retrocyclins on HIV-1 and HSV may result from the ability to prevent viral entry (*5*). More recently, Leikina et al. (*6*) demonstrated that retrocyclins can also prevent the entry of influenza A virus into target cells. Since this anti-influenza activity resulted from the ability of retrocyclins to bind *and cross-link* cell-surface glycoproteins of the target cell or the viral fusion protein (hemagglutinin), the formation of oligomers is likely to be an essential component of retrocyclin-mediated antiviral activity.

In summary, we have shown that the structure of retrocyclin-2 is stabilized in the presence of micelles and that it self-associates in a concentration-dependent manner in aqueous solution to form a trimer. The interactions observed for retrocyclin-2 with membrane environments are thought to be important for biological activity (*33*), and the current study has provided the first 3D structure of a θ-defensin in a membrane-mimicking environment. The structure determined here for retrocyclin-2 may be useful in further elucidation of the mechanism of action of θ-defensins.

ACKNOWLEDGMENT

The authors thank Paramjit Bansal for helpful discussions.

REFERENCES

1. Cole, A. M., Hong, T., Boo, L. M., Nguyen, T., Zhao, C., Bristol, G., Zack, J. A., Waring, A. J., Yang, O. O., and Lehrer, R. I. (2002) Retrocyclin: a primate peptide that protects cells from infection by T- and M-tropic strains of HIV-1, *Proc. Natl. Acad. Sci. U.S.A. 99*, 1813−1818.
2. Owen, S. M., Rudolph, D. L., Wang, W., Cole, A. M., Waring, A. J., Lal, R. B., and Lehrer, R. I. (2004) RC-101, a retrocyclin-1 analogue with enhanced activity against primary HIV type 1 isolates, *AIDS Res. Hum. Retroviruses 20*, 1157−1165.
3. Owen, S. M., Rudolph, D., Wang, W., Cole, A. M., Sherman, M. A., Waring, A. J., Lehrer, R. I., and Lal, R. B. (2004) A theta-defensin composed exclusively of D-amino acids is active against HIV-1, *J. Pept. Res. 63*, 469−476.
4. Wang, W., Owen, S. M., Rudolph, D. L., Cole, A. M., Hong, T., Waring, A. J., Lal, R. B., and Lehrer, R. I. (2004) Activity of alpha- and theta-defensins against primary isolates of HIV-1, *J. Immunol. 173*, 515−520.
5. Yasin, B., Wang, W., Pang, M., Cheshenko, N., Hong, T., Waring, A. J., Herold, B. C., Wagar, E. A., and Lehrer, R. I. (2004) θ-Defensins protect cells from infection by herpes simplex virus by inhibiting viral adhesion and entry, *J. Virol. 78*, 5147−5156.
6. Leikina, E., Delanoe-Ayari, H., Melikov, K., Cho, M. S., Chen, A., Waring, A. J., Wang, W., Xie, Y., Loo, J. A., Lehrer, R. I., and Chernomordik, L. V. (2005) Carbohydrate-binding molecules inhibit viral fusion and entry by crosslinking membrane glycoproteins, *Nat. Immunol. 6*, 995−1001.
7. Wang, W., Mulakala, C., Ward, S. C., Jung, G., Luong, H., Pham, D., Waring, A. J., Kaznessis, Y., Lu, W., Bradley, K. A., and Lehrer, R. I. (2006) Retrocyclins kill bacilli and germinating spores of *Bacillus anthracis* and inactivate anthrax lethal toxin, *J. Biol. Chem. 281*, 32755−32764.
8. Cole, A. L., Herasimtschuk, A., Gupta, P., Waring, A. J., Lehrer, R. I., and Cole, A. M. (2007) The retrocyclin analogue RC-101 prevents human immunodeficiency virus type 1 infection of a model human cervicovaginal tissue construct, *Immunology 121*, 140−145.
9. Tang, Y.-Q., Yuan, J., Ösapay, G., Ösapay, K., Tran, D., Miller, C. J., Ouellette, A. J., and Selsted, M. E. (1999) A cyclic antimicrobial peptide produced in primate leukocytes by the ligation of two truncated α-defensins, *Science 286*, 498−502.
10. Nguyen, T. X., Cole, A. M., and Lehrer, R. I. (2003) Evolution of primate theta-defensins: a serpentine path to a sweet tooth, *Peptides 24*, 1647−1654.
11. Wang, W., Cole, A. M., Hong, T., Waring, A. J., and Lehrer, R. I. (2003) Retrocyclin, an antiretroviral theta-defensin, is a lectin, *J. Immunol. 170*, 4708−4716.
12. Gallo, S. A., Wang, W., Rawat, S. S., Jung, G., Waring, A. J., Cole, A. M., Lu, H., Yan, X., Daly, N. L., Craik, D. J., Jiang, S., Lehrer, R. I., and Blumenthal, R. (2006) Theta-defensins prevent HIV-1 Env-mediated fusion by binding gp41 and blocking 6-helix bundle formation, *J. Biol. Chem. 281*, 18787−18792.
13. Trabi, M., Schirra, H. J., and Craik, D. J. (2001) Three-dimensional structure of RTD-1, a cyclic antimicrobial defensin from *Rhesus macaque* leukocytes, *Biochemistry 40*, 4211−4221.
14. Fields, C. G., Lloyd, D. H., Macdonald, R. L., Otteson, K. M., and Noble, R. L. (1991) HBTU activation for automated Fmoc solid-phase peptide synthesis, *Pept. Res. 4*, 95−101.
15. Chan, W. C., and White, P. D. (2000) *Fmoc Solid Phase Peptide Synthesis*, Oxford University Press Inc., New York.
16. Marion, D., and Wüthrich, K. (1983) Application of phase sensitive two-dimensional correlated spectroscopy (COSY) for measurements of ^{1}H-^{1}H spin-spin coupling constants in proteins, *Biochem. Biophys. Res. Commun. 113*, 967−974.
17. Braunschweiler, L., and Ernst, R. R. (1983) Coherence transfer by isotropic mixing: application to proton correlation spectroscopy, *J. Magn. Reson. 53*, 521−528.
18. Bax, A., and Davis, D. G. (1985) MLEV-17-based two-dimensional homonuclear magnetization transfer spectroscopy, *J. Magn. Reson. 65*, 355−360.
19. Rance, M., Sørensen, O. W., Bodenhausen, G., Wagner, G., Ernst, R. R., and Wüthrich, K. (1983) Improved spectral resolution in COSY ^{1}H NMR spectra of proteins via double quantum filtering, *Biochem. Biophys. Res. Commun. 117*, 479−485.
20. Griesinger, C., Sørensen, O. W., and Ernst, R. R. (1987) Practical aspects of the E. COSY technique, measurement of scalar spin-spin coupling constants in peptides, *J. Magn. Reson. 75*, 474−492.
21. Jeener, J., Meier, B. H., Bachmann, P., and Ernst, R. R. (1979) Investigation of exchange processes by two-dimensional NMR spectroscopy, *J. Chem. Phys. 71*, 4546−4553.

22. Piotto, M., Saudek, V., and Sklenar, V. (1992) Gradient-tailored excitation for single-quantum NMR spectroscopy of aqueous solutions, *J. Biomol. NMR 2*, 661−665.
23. Altieri, A. S., Hinton, D. P., and Byrd, R. A. (1995) Association of Biomolecular systems via pulsed field gradient NMR self-diffusion measurements, *J. Am. Chem. Soc. 117*, 7566−7567.
24. Wilkins, D. K., Grimshaw, S. B., Receveur, V., Dobson, C. M., Jones, J. A., and Smith, L. J. (1999) Hydrodynamic radii of native and denatured proteins measured by pulse field gradient NMR techniques, *Biochemistry 38*, 16424−16431.
25. Guntert, P., Mumenthaler, C., and Wüthrich, K. (1997) Torsion angle dynamics for NMR structure calculation with the new program DYANA, *J. Mol. Biol. 273*, 283−298.
26. Brünger, A. T., Adams, P. D., and Rice, L. M. (1997) New applications of simulated annealing in X-ray crystallography and solution NMR, *Structure 5*, 325−336.
27. Rice, L. M., and Brünger, A. T. (1994) Torsion angle dynamics: reduced variable conformational sampling enhances crystallographic structure refinement, *Proteins 19*, 277−290.
28. Stein, E. G., Rice, L. M., and Brünger, A. T. (1997) Torsion-angle molecular dynamics as a new efficient tool for NMR structure calculation, *J. Magn. Reson. 124*, 154−164.
29. Linge, J. P., and Nilges, M. (1999) Influence of non-bonded parameters on the quality of NMR structures: a new force field for NMR structure calculation, *J. Biomol. NMR 13*, 51−59.
30. Hutchinson, E. G., and Thornton, J. M. (1996) PROMOTIF-A program to identify and analyze structural motifs in proteins, *Protein Sci. 5*, 212−220.
31. Laskowski, R. A., Rullmannn, J. A., MacArthur, M. W., Kaptein, R., and Thornton, J. M. (1996) AQUA and PROCHECK-NMR: programs for checking the quality of protein structures solved by NMR, *J. Biomol. NMR 8*, 477−486.
32. Cohn, E. J., and Edsall, J. T. (1943) Density and Apparent Specific Volume of Proteins, in *Proteins, Amino Acids and Peptides as Ions and Dipolar Ions*, Reinhold Publishing Corporation, New York.
33. Tang, M., Waring, A. J., Lehrer, R. I., and Hong, M. (2006) Orientation of a β-hairpin antimicrobial peptide in lipid bilayers from two-dimensional dipolar chemical-shift correlation NMR, *Biophys. J. 90*, 3616−3624.
34. Moore, P. N., Puvvada, S., and Blankschtein, D. (2003) Challenging the surfactant monomer skin penetration model: penetration of sodium dodecyl sulfate micelles into the epidermis, *J. Cosmet. Sci. 54*, 29−46.
35. Cierpicki, T., and Otlewski, J. (2001) Amide proton temperature coefficients as hydrogen bond indicators in proteins, *J. Biomol. NMR 21*, 249−261.
36. Craik, D. J., Daly, N. L., Bond, T., and Waine, C. (1999) Plant cyclotides: a unique family of cyclic and knotted proteins that defines the cyclic cystine knot structural motif, *J. Mol. Biol. 294*, 1327−1336.
37. Craik, D. J., Daly, N. L., and Waine, C. (2001) The cystine knot motif in toxins and implications for drug design, *Toxicon 39*, 43−60.
38. Luckett, S., Garcia, R. S., Barker, J. J., Konarev, A. V., Shewry, P. R., Clarke, A. R., and Brady, R. L. (1999) High-resolution structure of a potent, cyclic proteinase inhibitor from sunflower seeds, *J. Mol. Biol. 290*, 525−533.
39. Korsinczky, M. L., Schirra, H. J., Rosengren, K. J., West, J., Condie, B. A., Otvos, L., Anderson, M. A., and Craik, D. J. (2001) Solution structures by ^{1}H NMR of the novel cyclic trypsin inhibitor SFTI-1 from sunflower seeds and an acyclic permutant, *J. Mol. Biol. 311*, 579−591.
40. Abuja, P. M., Zenz, A., Trabi, M., Craik, D. J., and Lohner, K. (2004) The cyclic antimicrobial peptide RTD-1 induces stabilized lipid-peptide domains more efficiently than its open-chain analogue, *FEBS Lett. 566*, 301−306.
41. Munoz, V., Ghirlando, R., Blanco, F. J., Jas, G. S., Hofrichter, J., and Eaton, W. A. (2006) Folding and aggregation kinetics of a beta-hairpin, *Biochemistry 45*, 7023−7035.
42. Pfuhl, M., Chen, H. A., Kristensen, S. M., and Driscoll, P. C. (1999) NMR exchange broadening arising from specific low affinity protein self-association: analysis of nitrogen-15 nuclear relaxation for rat CD2 domain 1, *J. Biomol. NMR 14*, 307−320.
43. Wishart, D. S., Bigam, C. G., Holm, A., Hodges, R. S., and Sykes, B. D. (1995) ^{1}H, ^{13}C and ^{15}N random coil NMR chemical shifts of the common amino acids. I. Investigations of nearest-neighbor effects, *J. Biomol. NMR 5*, 67−81.
44. Rosengren, K. J., Daly, N. L., Plan, M. R., Waine, C., and Craik, D. J. (2003) Twists, knots, and rings in proteins. Structural definition of the cyclotide framework, *J. Biol. Chem. 278*, 8606−8616.

BI700720E